Journal of Power Sources 195 (2010) 393–401

Contents lists available at ScienceDirect

Journal of Power Sources

journal homepage: www.elsevier.com/locate/jpowsour

# Comparative study of doped ceria thin-film electrolytes prepared by wet powder spraying with powder synthesized via two techniques

Huangang Shi, Wei Zhou, Ran Ran, Zongping Shao*

*State Key Laboratory of Materials-Oriented Chemical Engineering, College of Chemistry & Chemical Engineering, Nanjing University of Technology, No. 5 Xin Mofan Road, Nanjing 210009, PR China*

ARTICLE INFO

*Article history:*
Received 10 July 2009
Received in revised form 31 July 2009
Accepted 31 July 2009
Available online 8 August 2009

*Keywords:*
Samaria-doped ceria
Thin-film electrolyte
Solid-oxide fuel cells
Fabrication

ABSTRACT

Fabrication of dense $Sm_{0.2}Ce_{0.8}O_{1.9}$ (SDC) thin-film electrolytes by wet powder spraying in combination with high-temperature sintering is investigated. Two powder synthesis techniques, *i.e.*, a hydrothermal synthesis and an EDTA–citrate complexing sol–gel process, were investigated. X-ray diffraction, BET surface area and laser particle size analysis demonstrate there is certain level of aggregation in both powders. However, it is more pronounced in powders obtained by the complexing process, and only the colloidal suspensions of powders prepared by hydrothermal synthesis are stable. SEM analysis of the green and sintered thin-film electrolytes demonstrate that the SDC electrolyte with powders prepared via the hydrothermal synthesis is denser. By optimizing the fabrication conditions, dense SDC electrolytes with a thickness of ~12 μm are successfully fabricated. The cells with SDC prepared from hydrothermal synthesis demonstrate open circuit voltages and power outputs similar to those of similar cells fabricated from other advanced techniques. Because of its simplicity and flexibility for anode substrate geometric shape, it turns out to be a promising technology to fabricate thin-film SDC electrolyte for solid-oxide fuel cell application.



## 1. Introduction

There is increasing interest in decreasing operating temperatures of solid-oxide fuel cells (SOFCs) from ~1000 °C to the intermediate-to-low temperature range of 400–800 °C [1,2]. Such decreases would provide several benefits, including more flexibility in cell material selection, reduced fabrication and operating costs, prolonged lifetime by suppressing interfacial reactions between cell components and better sealing. However, practical problems are associated with reductions in the operating temperature of traditional SOFCs based on thick yttria-stabilized zirconia (YSZ) electrolytes and $La_{0.8}Sr_{0.2}MnO_3$ (LSM) perovskite cathodes. For example, it causes a sharp increase in electrolyte ohmic resistance and electrode polarization resistance.

For hydrogen fueled SOFCs, the cathode was found to be the main contributor to electrode polarization resistance. Thereby, considerable research efforts have focused on improving the electrocatalytic activity of the cathode for oxygen reduction at low temperature [3,4]. Many new cathode materials have been successfully developed including mixed oxygen-ionic and electronic conducting oxides of $Ba_{0.5}Sr_{0.5}Co_{0.8}Fe_{0.2}O_{3-\delta}$ (BSCF) [5,6], $La_{0.6}Sr_{0.4}Co_{0.8}Fe_{0.2}O_{3-\delta}$ (LSCF) [7–9] and $Sm_{0.5}Sr_{0.5}CoO_{3-\delta}$ (SSC) [10–12], and precious metal (Ag/Pt/Pd) modified oxide electrodes [13–19]. Cathodic polarization resistance as low as 0.1 Ω cm$^2$ has been reported at 600 °C [20–23].

Electrolyte ohmic resistance must also be minimized to achieve high cell performance at intermediate-to-low temperatures. To this end, the electrolyte thickness can be reduced or new electrolyte materials with higher ionic conductivity can be developed [24,25]. YSZ are the most widely used solid electrolytes in high-temperature SOFCs. Samaria or gadolinia doped ceria (SDC, GDC) have much higher ionic conductivity than YSZ at reduced temperatures [26,27]. Although doped ceria display significant electronic conductivity at high temperature, their electronic transfer number decreases quickly with decreasing operating temperature. It is generally believed that doped ceria could potentially serve as electrolytes for IT-SOFCs operating at temperatures lower than 650 °C [28]. On the other hand, Steele et al. pointed out that area specific ohmic resistance of the electrolyte needs to be reduced less than 0.15 Ω cm$^2$ to achieve power output of practical importance [29]. It suggests doped ceria electrolytes need also to be in a thin-film configuration to operate them at temperatures lower than 650 °C.

When the electrolyte membrane thickness is reduced to tens of micrometers, it should be mechanically supported with an underlying substrate. Anode-supported thin-film electrolyte configurations are most frequently adopted up to now. A number of coating techniques such as chemical vapor deposition (CVD) [30], physical vapor deposition (PVD) [31], electrochemical vapor

* Corresponding author. Tel.: +86 25 83172256; fax: +86 25 83172256.
*E-mail address:* shaozp@njut.edu.cn (Z. Shao).

0378-7753/$ – see front matter © 2009 Elsevier B.V. All rights reserved.
doi:10.1016/j.jpowsour.2009.07.056

deposition (EVD) [32], and ceramic powder processes can generate thin-film electrolytes on porous substrates for SOFC applications. Ceramic powder processes, including tape casting [33], electrophoretic deposition [34] and screen-printing [35], have received considerable attention recently because they are low in cost, efficient and easy to scale up. However, these processes can only be used for flat cells. Dual dry pressing is frequently used when performing research in a laboratory setting [36–38], but is applicable only for coin-size flat cells. Wet powder spraying (WPS) [39], sometimes called suspension spraying [40], is a non-contact technique that can be used for flat substrates, corrugated sheets, tubes and a variety of other substrates. It is also easy to scale up wet powder spraying from laboratory to industrial fabrication.

We have previously reported the fabrication of an anode-supported thin-film YSZ electrolyte for SOFCs via wet powder spraying with powder synthesized by an EDTA–citrate complexing sol–gel process [41]. Both powder aggregation and the presence of organics in the substrate were found to have a significant effect on the quality and densification of the thin electrolyte layer. The aggregation can be eliminated by high-energy ball milling. In addition, the powder synthesis technique could greatly influence the powder properties such as surface area, phase purity, aggregation, particle size, particle size distribution and conductivity. As a result, powder synthesis may also affect the sintering and performance of a thin-film electrolyte prepared via wet powder spraying [42–46].

As part of our efforts to reduce the operating temperature of SOFCs to below 600 °C, the fabrication of anode-supported thin-film SDC electrolytes by wet powder spraying was exploited. As compared to YSZ electrolytes, $CeO_2$-based electrolytes are more difficult to densify. Many researches are focused on the sinterability of the doped ceria electrolytes at reduced temperatures [47–50]. In this study, special attention was paid to the effect of different powder synthesis techniques on the densification of SDC electrolytes and the consequent cell performance.

## 2. Experimental

### 2.1. Synthesis

All the raw materials used in this study were obtained from Sinopharm Chemical Reagent Co. Ltd., Shanghai China in analytical grade. Two wet-chemical techniques were used for the synthesis of $Ce_{0.8}Sm_{0.2}O_{1.9}$ (SDC) powders for wet powder spraying deposition, *i.e.*, hydrothermal synthesis and a combined EDTA–citrate complexing sol–gel process.

#### 2.1.1. Hydrothermal synthesis

$Sm(NO_3)_3{\cdot}6H_2O$ and $Ce(NO_3)_3{\cdot}6H_2O$ raw materials were mixed into a solution with 0.8 M $Ce^{3+}$ and 0.2 M $Sm^{3+}$. Ammonia was used to adjust the pH value of the solution to ~10. After stirring at room temperature for ~30 min, the brown-colored solution was transferred into a Teflon-lined autoclave (100-ml capacity). The sealed autoclave was kept in an electric oven at 180 °C for 24 h and water-cooled to room temperature. The bright yellow products were filtered, washed with deionized water several times, dried and calcined at 800 °C for 5 h in air. The SDC powders obtained via hydrothermal synthesis are referred to as SDC-HT.

#### 2.1.2. Combined EDTA–citrate sol–gel process

The synthesis of SDC powder by an EDTA–citrate complexing method has been described in detail in our previous publication [51]. In brief, stoichiometric amounts of $Sm(NO_3)_3{\cdot}6H_2O$ and $Ce(NO_3)_3{\cdot}6H_2O$ (according to the molecular composition of the oxide) were mixed into a solution. EDTA and citric acid were then added as the complexing agents. The mole ratio of EDTA to citric acid to total metal ions was set at 1:2:1. $NH_3{\cdot}H_2O$ was used to adjust the pH value of the solution to ~6. Water was evaporated from the solution while stirring at 90 °C, creating transparent gels that were fired at 250 °C and calcined at 800 °C for 5 h in air. The SDC powders obtained with this technique are referred to as SDC-EC.

$Ba_{0.5}Sr_{0.5}Co_{0.8}Fe_{0.2}O_{3-\delta}$ (BSCF), the cathode material, was also synthesized with an EDTA–citrate complexing sol–gel process. The primary powder from pre-firing the gel at 250 °C was calcined at 900 °C for 5 h in air. The powder was then used for cathode layer preparation.

### 2.2. Fabrication

#### 2.2.1. Anode substrates

The anode substrates were prepared by a dry pressing/sintering process. Nickel oxide, SDC-EC (800 °C calcined) and polyvinyl butyral (PVB) were well mixed at a weight ratio of 57:38:5 with an agate mortar and pestle. The mixed powder was then pressed into disk-shape pellets using a 15 mm stainless steel die under a hydraulic pressure of 200 MPa for 1 min. These green pellets were sintered at 1000 °C in air for 5 h to remove organic substances and sinter the particles, ensuring sufficient mechanical strength for subsequent electrolyte deposition.

#### 2.2.2. Fabrication of the electrolyte layer by wet powder spraying

The as-synthesized SDC powders (SDC-HT and SDC-EC) were suspended in ethylene glycol (EG) in an 80 ml zirconia container and agitated on a high-energy ball miller (Model Pulverisette 6, Fritsch, Germany) at 500 rpm for 1 h. The weight percentage of SDC powder in the colloidal suspensions was about 5%. To fabricate the thin-film SDC, the colloidal suspension was sprayed with 1 atm nitrogen gas onto the anode substrate using a modified spraying gun (BD-128, Fenghua Bida Machinery Manufacture Co. Ltd., China) with a nozzle size of 0.35 mm (pore diameter). The spray gun was aligned above the heated anode substrate (250 °C on a hot plate) at a distance of 10 mm. The effective deposition speed calculated was about 0.005 g $cm^{-2}$ $min^{-1}$ SDC. The two layer cells were then fired at 1500 °C in air for 5 h at a heating and cooling rate of 5 °C $min^{-1}$.

#### 2.2.3. Deposition of the cathode layer

To form a complete single cell, the BSCF colloidal suspension, prepared in the same way as the SDC suspension, was sprayed onto the center of the electrolyte through a high-temperature plastic mask with a 6 mm diameter, creating an effective surface area of ~0.48 $cm^2$. The three-layer cells were fired at 1000 °C for 2 h to make the cathode layer adhere firmly to the electrolyte surface and create strong connections between BSCF particles.

### 2.3. Basic characterization

The phase composition of the powders was analyzed by X-ray diffraction (XRD, Bruker D8 Advance, Germany) using Cu Kα radiation (λ = 1.5418 Å) at room temperature. Specific surface areas of the synthesized SDC powders were measured at liquid nitrogen temperatures using a nitrogen adsorption–desorption instrument (BEL SORP II, Ankersmid Company, Netherlands). For both SDC colloidal suspensions, particle size and distribution were measured with a laser particle size analyzer (LPSA, Microtrac S3500, America). The fuel cell morphologies were observed using an environmental scanning electron microscope (ESEM, Model QUANTA-2000, FEI Company, Hillsboro, OR).

SDC conductivity was measured via electrochemical impedance spectroscopy (EIS). SDC powders were die-pressed into approximately 1-mm thick pellets and sintered at 1500 °C for 5 h. Both pellet surfaces were painted with silver pastes as electrodes. Silver wires attached to the electrodes were used as current collectors. Impedance spectroscopy was measured with a Solartron 1260A

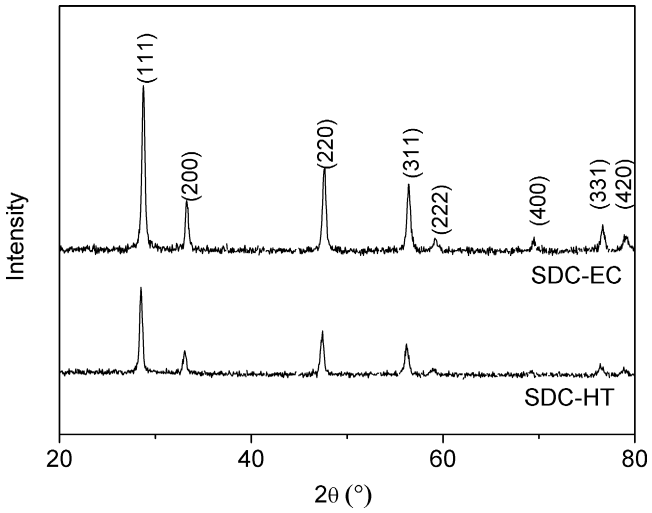


**Fig. 1.** X-ray diffraction patterns of the synthesized SDC powders.

frequency response analyzer. Measurement was performed in air between 400 and 700 °C at 50 °C intervals in a frequency range of $10^6$ to 1 Hz with signal amplitude of 10 mV.

### 2.4. Fuel cell test

An in-lab constructed fuel cell test station was used to evaluate the electrochemical performance of the fabricated cells. The fuel cell was sealed onto a quartz tube using silver paste to form an anode chamber, which was then heated to 600 °C at a rate of 2 °C $min^{-1}$ and held for 5 h to set the seal. Hydrogen at a flow rate of 20 ml $min^{-1}$ [STP] was introduced into the anode chamber to begin in situ reduction of anodic NiO to metallic nickel. After about 5 h, the hydrogen flow rate was increased to 80 ml $min^{-1}$ [STP] and bubbled through water at 25 °C for *I–V* cell polarization test. During the test, the cathode was exposed to the ambient atmosphere. *I–V* curves were collected at 50 °C intervals over a temperature range of 450–600 °C using a digital source meter (model 2420, Keithley, Cleveland, OH) with a four-probe configuration. EIS of the cell under open circuit voltage (OCV) conditions were measured with an electrochemical workstation comprised of a Solartron 1260A frequency response analyzer with a Solartron 1287 potentiostat. EIS were recorded in a frequency range of 10 kHz to 0.1 Hz with signal amplitude of 10 mV.

## 3. Results and discussion

### 3.1. Powder properties

Fig. 1 shows the X-ray diffraction patterns of the synthesized SDC-HT and SDC-EC powders (after the calcination at 800 °C in air for 5 h). The diffraction peaks in both samples can be indexed on a fluorite-type structure with cubic lattice symmetry. As listed in Table 1, the lattice constant (*a*), calculated with the unitcell program, was 0.5429 nm for SDC-EC and 0.5428 nm for SDC-HT. Because $Sm^{3+}$ is larger than $Ce^{4+}$, incorporating $Sm^{3+}$ into the structure of $CeO_2$ should expand the lattice. According to JCPDS card No.75-0157, 75-0158 and 75-0159, the lattice constants for

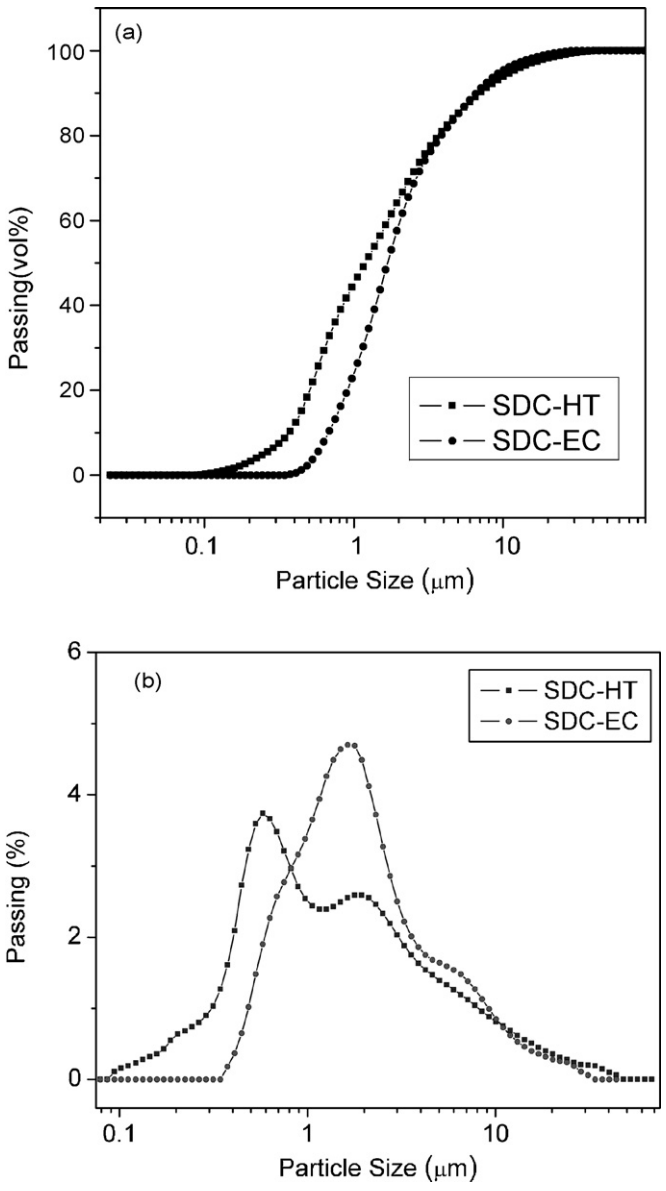


**Fig. 2.** Particle size and size distributions of the two powders.

$Sm_{0.1}Ce_{0.9}O_{1.95}$, $Sm_{0.2}Ce_{0.8}O_{1.9}$ and $Sm_{0.3}Ce_{0.7}O_{1.85}$ are 0.5423, 0.5433, and 0.5443 nm, respectively. The lattice constants of SDC-HT and SDC-EC best matched the lattice constant of $Sm_{0.2}Ce_{0.8}O_{1.9}$, indicating that a solid solution was successfully formed in both samples. SDC-EC oxide diffraction peaks showed much higher intensity than those of SDC-HT oxide even though both oxides were calcined at the same temperature (800 °C) for 5 h. This suggested that the sol–gel process resulted in improved oxide crystallinity. Oxide crystalline sizes were calculated based on the half peak width of the diffraction peak at miller index (1 1 1) using the Scherrer's equation:

$$D = \frac{0.9\lambda}{B\cos\theta}, \quad (1)$$

**Table 1**
Lattice constant, specific surface area and average crystallite size of the SDC powders prepared by hydrothermal method or EDTA–CA complexing sol–gel process.

| Powders | Lattice constant *a* (nm) | Average grain size $D_{XRD}$ (nm) | Specific surface area $S_{BET}$ ($m^2\ g^{-1}$) | Average grain size $D_{BET}$ (nm) |
|---|---|---|---|---|
| SDC-EC | 0.5429 | 22.8 | 12.2 | 68.8 |
| SDC-HT | 0.5428 | 19.5 | 23.1 | 36.4 |

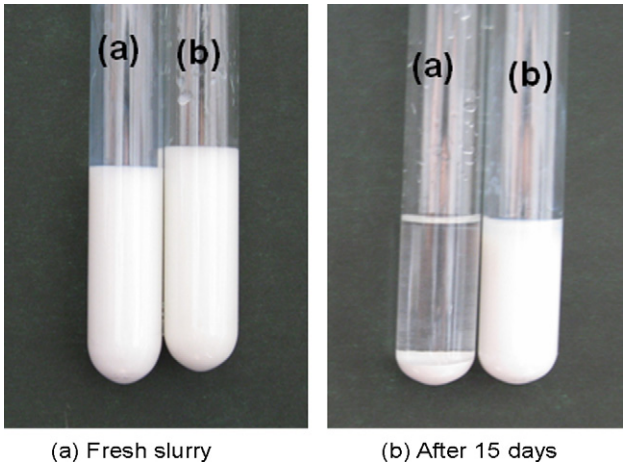


**Fig. 3.** Photos of the SDC suspensions freshly prepared and aged for 15 days ((a) for SDC-EC and (b) for SDC-HT).

where $D$ is the crystal size (nm), $\lambda$ is the X-ray wavelength (0.151418 nm), $\theta$ is the Bragg's diffraction angle (°) and $B$ is the half peak width (radian). As shown in Table 1, the calculated crystal sizes of SDC-HT and SDC-EC were 19.5 and 22.8 nm, respectively. That is, the hydrothermal process created slightly smaller crystals than the sol–gel process. Specific surface area was also measured. It is 23.1 $m^2\,g^{-1}$ for SDC-HT and 12.2 $m^2\,g^{-1}$ for SDC-EC. Assuming a spherical particle shape, the average powder grain size ($D_{BET}$) was calculated based on the equation:

$$D_{BET} = \frac{6}{\rho \cdot S_{BET}}, \quad (2)$$

where $\rho$ is the theoretical density of the oxide (7.15 g $cm^{-3}$), and $S_{BET}$ is the measured specific surface area of the oxide ($m^2\,g^{-1}$). SDC-HT had an average grain size of 36.4 nm, and SDC-EC had an average grain size of 68.8 nm, suggesting that, although there was aggregation in both samples, the sample prepared from the EDTA–citrate complexing sol–gel process aggregated more. One possible explanation for such differences is that the actual temperature during the high-temperature calcination for SDC-EC samples may have exceeded the set temperature (furnace temperature) because of considerable amounts of organics in the precursor that produced heat during the calcination.

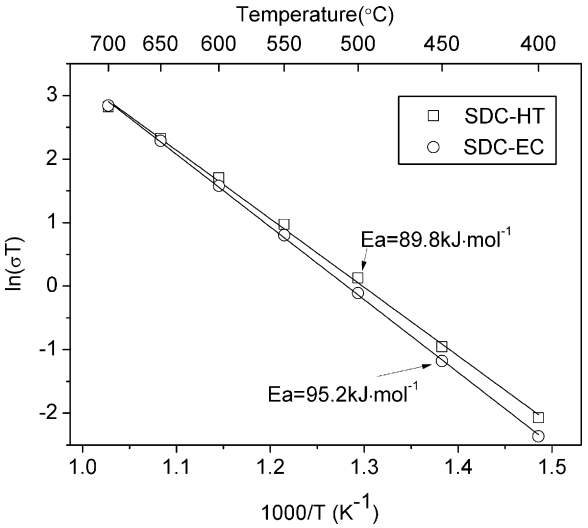


**Fig. 4.** Arrhenius plots of conductivity of SDC sintered at 1500 °C.

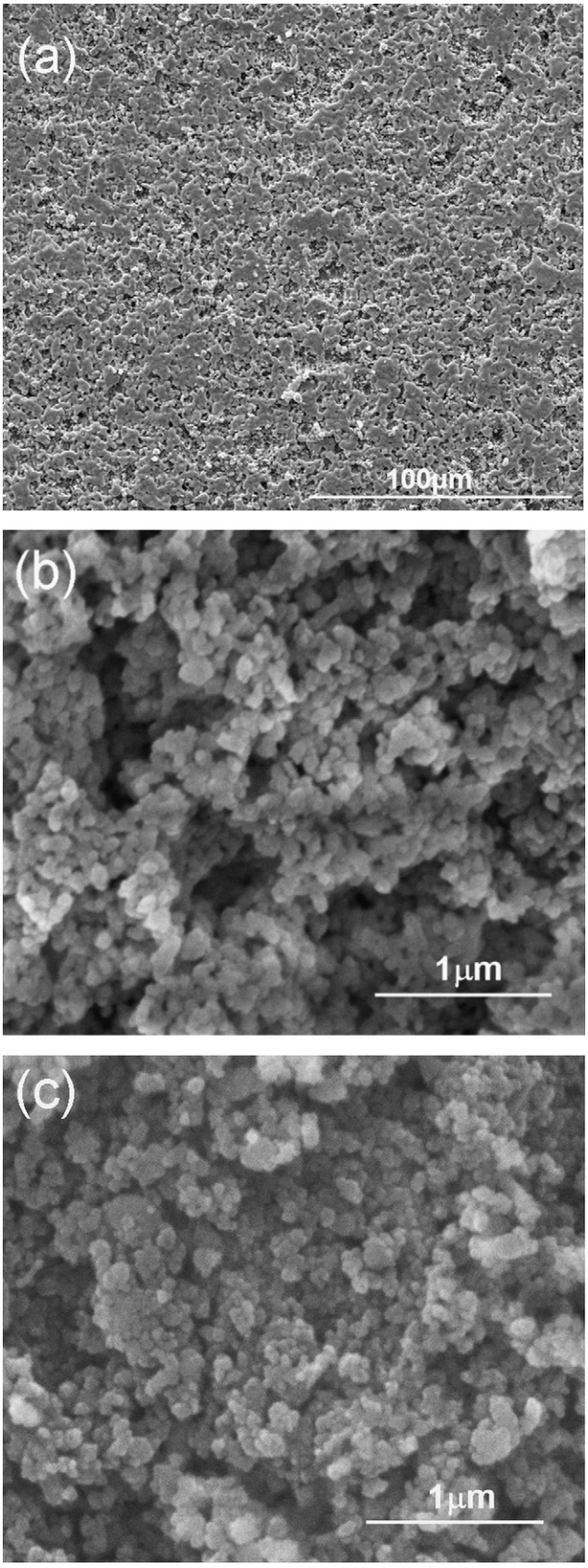


**Fig. 5.** SEM images of the anode substrate (a) and the sprayed green SDC layers ((b) for SDC-EC and (c) for SDC-HT).

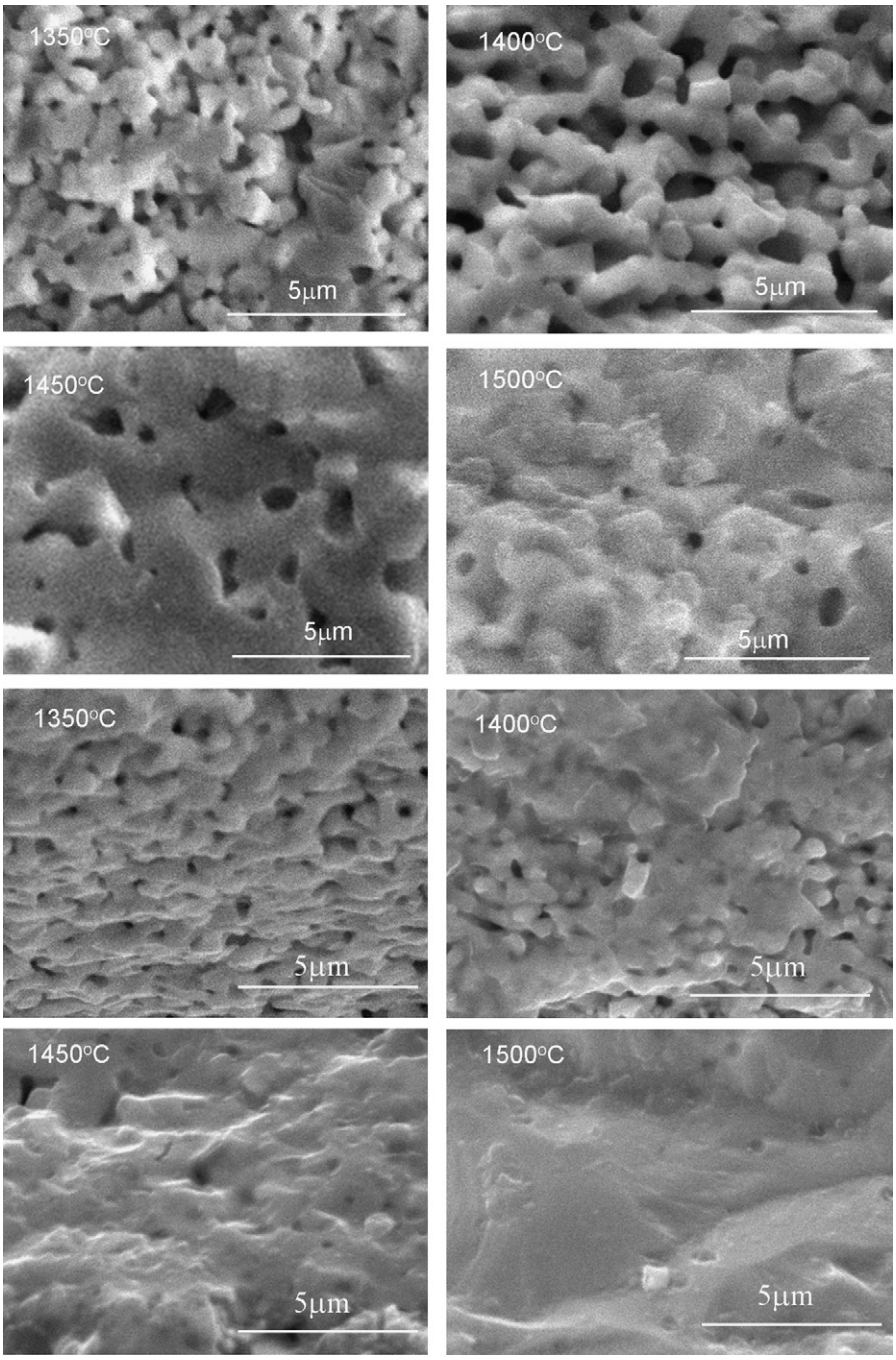


**Fig. 6.** SEM images of the cross-section morphologies of the electrolyte thin films with SDC-EC (a) and SDC-HT (b) sintered at different temperature.

The powders must be in a colloidal suspension to create thin-film electrolytes by the wet powder spraying technique. Since we had previously found that ethylene glycol (EG) was an effective liquid medium for YSZ powders, we also used EG in this study for SDC. Synthesized SDC powders were mixed into EG with a high-energy ball mill, homogeneously distributing the powders in the liquid to form colloidal suspensions and breaking-up soft aggregation and some hard aggregation. Fig. 2 shows the particle size and size distributions of the two powders after the ball milling at 500 rpm for 1 h. SDC-HT displays a bimodal particle distribution, with peaks around 0.6 and 2 μm. About 45 vol.% of the particles were smaller than 1 μm. SDC-EC particle distribution was also bimodal, with peaks around 2 and 5 μm. The volumetric percentage of particles smaller than 1 μm was only 25%. These results suggested that SDC-EC had more aggregation than SDC-HT even after the high-energy ball milling. Beckel et al. argued that electrolyte films prepared by ceramic powder processes are greatly limited by particle diameter in the suspension [42]. Therefore, the SDC-HT suspension was considered a better choice than the SDC-EC suspension for WPS.

Fig. 3 shows freshly prepared colloidal suspensions and suspensions aged at room temperature for 15 days. After the aging, the SDC-HT suspension did not display any sedimentation, while the SDC-EC particles separated from the EG liquid. The high stability of the SDC-HT colloidal suspension was attributed to its fine particle sizes, which resisted sedimentation by Brownian motion. Because of the high degree of SDC-EC aggregation, Brownian forces were not enough to prevent sedimentation. As demonstrated in our previous publication, colloidal suspension aggregation in wet pow-

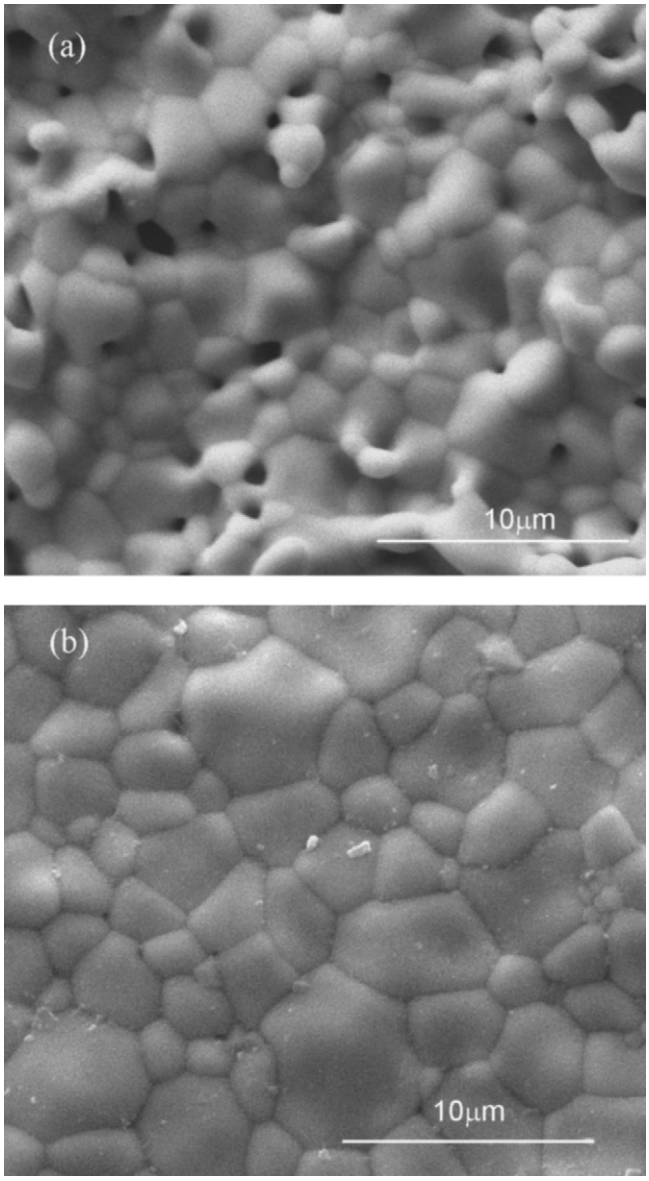


**Fig. 7.** SEM images of the SDC membranes after sintering at 1500 °C for 5 h ((a) for SDC-EC and (b) for SDC-HT).

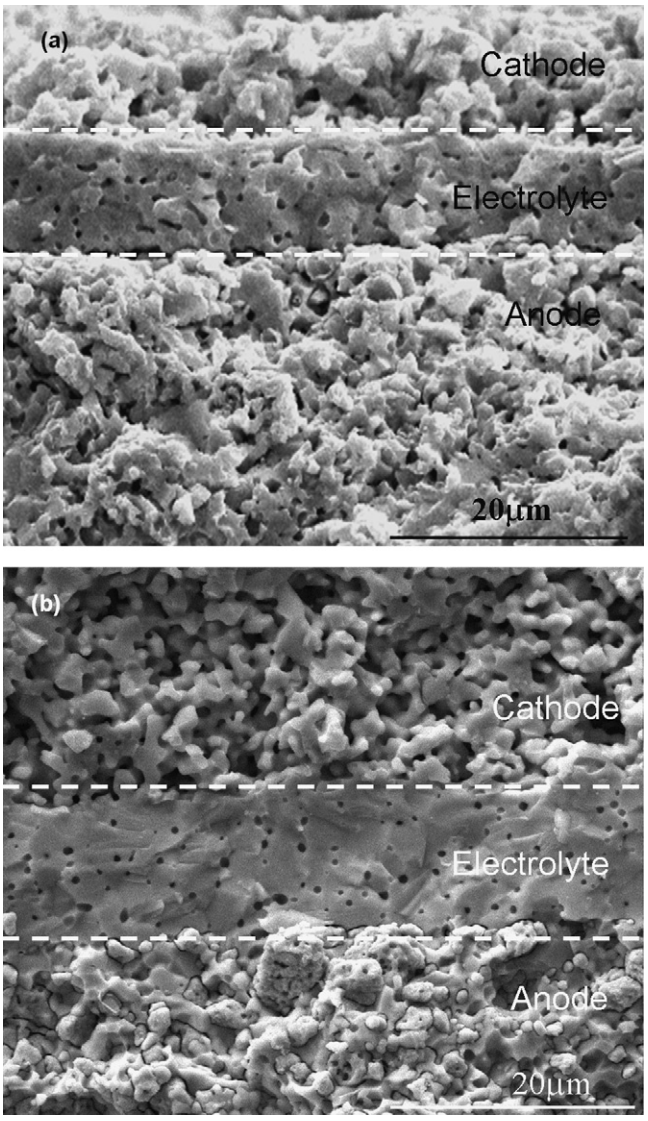


**Fig. 8.** SEM images of the cross-sectional morphologies of the cells ((a) for SDC-EC and (b) for SDC-HT).

der spraying processes could seriously impact the densification of YSZ thin films during high-temperature sintering processes [41]. In this respect, hydrothermal method is superior to the EDTA–citrate complexing sol–gel process for synthesizing SDC powders for wet powder spraying.

It is well known that synthesis technique also affects the electrical conductivity of many conducting oxides, especially doped ceria electrolytes [52]. Reported SDC electrical conductivity has ranged from $10^{-4}$ to $10^{-2}$ S cm$^{-1}$ at 600 °C in air [43–55]. Different synthesis techniques can result in different impurity levels and different grain morphologies, leading to different conductivities. Impurities, especially $SiO_2$, could significantly impact the ionic conductivity of SDC. $SiO_2$ can accumulate at grain boundaries by sedimentation from the oxide bulk during high-temperature sintering and block ionic transportation between grains [56]. The electrical conductivity of SDC-HT and SDC-EC were measured via electrochemical impedance spectroscopy (EIS). The powders were pressed into disk-shaped pellets under a hydraulic pressure of 400 MPa and sintered at 1500 °C in air for 5 h. Both surfaces of the pellets were painted with silver electrodes. Fig. 4 shows the electrical conductivity temperature dependence of SDC-HT and SDC-EC in an Arrhenius plot between 400 and 700 °C. The activation energy (Ea) for oxygen transportation was calculated with the equation:

$$\sigma_T = Ae^{-\mathrm{Ea}/RT}, \quad (3)$$

where $\sigma_T$ is ionic conductivity (S cm$^{-1}$), $A$ is the pre-exponential factor, $e$ is the natural logarithm, Ea is the activation energy, $R$ is molar gas constant (8.3145 J mol$^{-1}$ K$^{-1}$) and $T$ is the absolute temperature (K). The measured electrical conductivity of SDC-HT and SDC-EC at 600 °C was 0.0063 and 0.0056 S cm$^{-1}$, respectively. SDC-HT showed slightly higher conductivity than SDC-EC at corresponding temperatures. The calculated Ea was $89.9 \pm 1.3$ for SDC-HT and $95.2 \pm 0.8$ kJ mol$^{-1}$ for SDC-EC. Our results agreed with those of Huang et al., who prepared SDC20 by a sol–gel method, and measured a conductivity of 0.005 S cm$^{-1}$ at 600 °C in air and activation energy of 93.6 kJ mol$^{-1}$ [55]. Using the Archimedes method, the relative densities of the pellets were measured: 96.2% for SDC-HT and 95.8% for SDC-EC. Therefore, it is unlikely that the differences in conductivity between SDC-HT and SDC-EC were from the variation in sintering density. During the sol–gel synthesis, large amounts of organics (EDTA and citric acid) were added, which may contain inorganic impurities such as $SiO_2$ that had a

detrimental effect on the oxygen-ion transportation in the SDC bulk. The conductivity of SDC-EC was only slightly smaller than the conductivity of SDC-HT, suggesting that few impurities were introduced with the organics during the EDTA–citrate complexing process.

### 3.2. Thin-film formation

The anode substrates calcined at 1000 °C were air brushed to remove weakly attached anode particles and then heated to around 250 °C with a hot plate with constant power output. SDC colloidal suspensions after high-energy ball milling were sprayed onto the heated anode substrates. The EG immediately vaporized, leaving solid packed SDC particles on the substrate. The thickness of the electrolyte layer was controlled by the spray time and spray speed.

Fig. 5 presents the surface morphologies of the anode substrates and the sprayed green SDC layers. The anode substrate surface (Fig. 5a) was relatively smooth, with pore sizes less than 5 μm. As shown in Fig. 5b and c, both electrolytes layers were composed of SDC grains with primary grain sizes ~0.2 μm. However, the surface of the SDC-EC was much rougher and contained large irregular cavities between 0.2 and 1.5 μm in size. This surface may have been created from the large aggregates in the SDC-EC colloidal suspension. The surface of SDC-HT thin film was much smoother and contained fewer cavities, suggesting that powder aggregation should be avoided during the preparation of thin films by spray deposition.

Fig. 6a and b shows the cross-sectional SEM images of the SDC membranes prepared by wet powder spraying with SDC-HT or SDC-HT slurry after sintered at different temperatures of 1350, 1400, 1450, 1500 °C for 5 h. The SDC membranes were porous when the sintering temperature was below 1400 °C. Some pores were still observed inside the SDC-EC electrolyte film when it was sintered even at 1500 °C for 5 h. While the SDC-HT membrane is highly densified and free of cracks after sintering at 1450 °C. It suggests hydrothermal synthesis of SDC powder can result in better sintering of the thin-film electrolyte. Fig. 7a and b shows the surface morphologies of the SDC membranes prepared by wet powder spraying after sintering at 1500 °C for 5 h. The SDC membranes derived from SDC-EC powder were composed of grains with the main size of 2–5 μm. Some pores (~1 μm in diameter) were also observed. The thin-film prepared from SDC-HT was well sintered with the main grain size of 3–4 μm. Fig. 8 presents the cross-sectional morphologies of the complete cells with the thin-film electrolyte prepared by wet powder spraying. SDC-EC and SDC-HT electrolyte layer thicknesses were 10 and 12 μm, respectively. Although many pores were seen in the electrolyte layer made from the SDC-EC powder, no penetrated pinholes was observed throughout the whole electrolyte layer. The thin film prepared from SDC-HT was much denser, as shown in Fig. 8b.

### 3.3. Cell performance

The electrochemical performance of the cells derived from SDC-EC and SDC-HT were measured by *I–V* polarization. Here, BSCF was selected as the cathode material. Pure hydrogen bubbled through water at 25 °C was the fuel, while the cathode was exposed to the ambient atmosphere. As shown in Fig. 9a, the cell prepared from SDC-EC generated open circuit voltages of 0.765, 0.787, 0.804 and 0.826 at 600, 550, 500 and 450 °C, respectively. These values are slightly lower than those for an anode-supported thin-film SDC electrolyte prepared by dual dry pressing reported by Shao et al. [5]. This may be in part due to a thinner electrolyte (~10 μm) of this study. The decrease in membrane thickness made the current leakage more significant. Alternatively, this could also in part due to less densification as compared with the electrolyte prepared

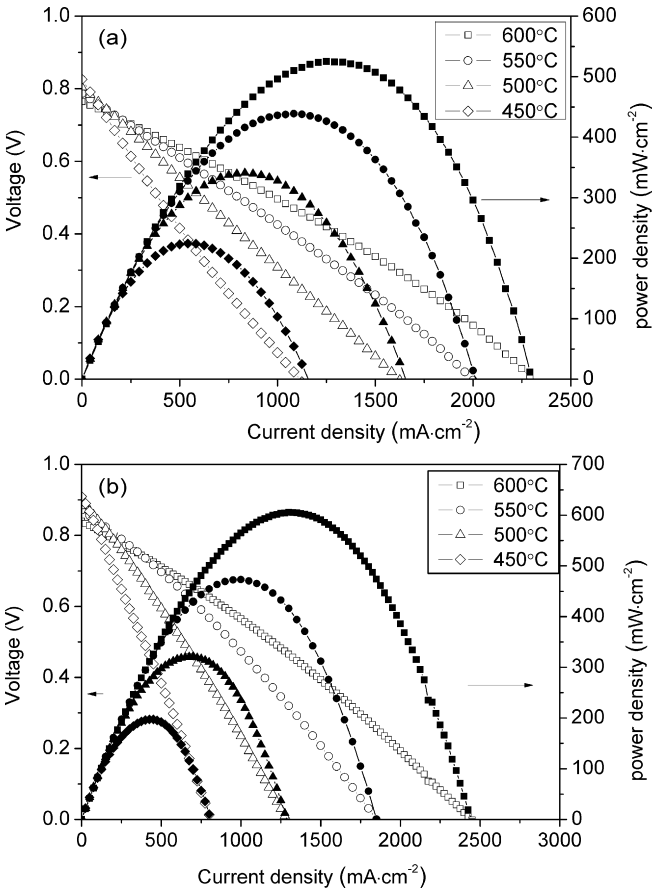


**Fig. 9.** Cell voltages (open symbols) and power densities (solid symbols) as a function of the current densities for the fuel cells ((a) for SDC-EC and (b) for SDC-HT).

by dual drying pressing. The cell derived from SDC-HT generated OCVs of 0.840, 0.872, 0.894, and 0.910 V at 600, 550, 500 and 450 °C, respectively. These values are slightly higher than the result with an anode-supported 10-μm SDC film prepared by tape casting reported by Zhang et al. [57] The higher OCVs of the cells from SDC-HT as compared to those of cells from SDC-EC is due to the better densification. However, both cells delivered promising power outputs. The peak power densities at 600 °C reached 525 and 605 mW cm$^{-2}$ for cells with SDC-EC and SDC-HT electrolyte, respectively. These results show the potential application of these films for SOFC at 600 °C. Thus, wet powder spraying is a promising technique for preparation of thin-film SDC electrolytes for reduced-temperature SOFCs.

Electrochemical impedance under open circuit voltage conditions at 600 °C was measured (Fig. 10) to get further information to interpret the better performance of the SDC-HT cell than SDC-EC cell. In both cells, the impedance spectroscopy showed a high frequency tail attributed to inductance from the cables and three depressed, overlapped semicircles. The impedance data were fitted to an equivalent circuit containing parallel resistor/constant phase element components and an inductor along with the series resistor as shown in Fig. 10 as an insert. The series resistance is the ohmic resistance that is somewhat lower than the high frequency intercept. The low-frequency intercept gives the total resistance ($R_{ohm} + R_p$), which includes the ohmic resistance of the cell, concentration polarization (mass-transfer or gas-diffusion polarization) resistance and the effective interfacial polarization resistances associated with the electrochemical reactions at both electrode–electrolyte interfaces (anode–electrolyte and cathode–electrolyte). The ohmic resistance and electrode

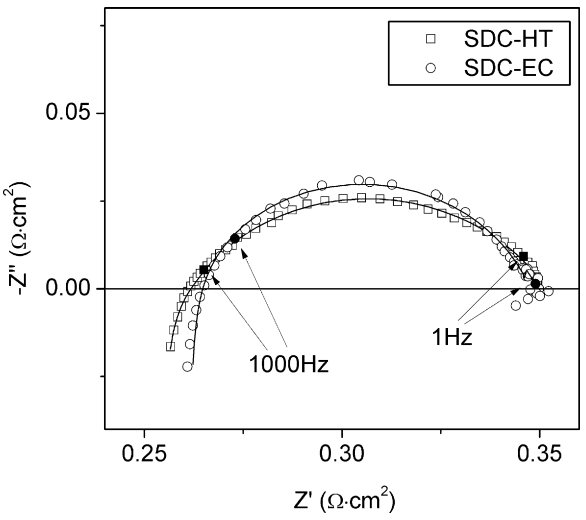


**Fig. 10.** EIS of the thin-film solid-oxide fuel cells at OCV conditions at 600 °C.

polarization resistance for SDC-HT cell and SDC-EC cell were 0.261/0.087 and 0.265/0.081 $\Omega\,cm^2$, respectively, suggesting that in both cells the electrolyte ohmic resistance overwhelmed the electrode polarization resistance. The nominal electrolyte conductivity was calculated based on the electrolyte ohmic resistance and the electrolyte thickness from Fig. 8. Nominal electrolyte conductivity was 4.5 and $3.8 \times 10^{-3}\,S\,cm^{-1}$ for SDC-HT and SDC-EC, respectively. These values are slightly lower than those measured with thick membranes. The differences were mainly a result of the thin-film membranes being less dense than the self-supported thick membranes. SDC-HT cell yielded a smaller polarization resistance than SDC-EC cell. It can be attributed to its higher density.

## 4. Conclusions

In this study, thin-film samaria-doped ceria electrolytes were fabricated by a ceramic powder process adopting a wet powder spraying technique for intermediate temperature solid-oxide fuel cell applications. The following conclusions can be derived:

(1) Wet powder spraying can be used to fabricate thin-film electrolyte membranes for fuel cell applications. However, the powder synthesis technique greatly impacts the density and performance of the thin-film electrolytes.
(2) Hydrothermal synthesis leads to less aggregation than the EDTA–citrate complexing sol–gel process. Powder aggregations decreased the density of the thin-film electrolytes.
(3) Under optimized fabrication conditions, the powders prepared by both EDTA–citrate complexing sol–gel process and hydrothermal synthesis were successfully used in the wet powder spraying process for the fabrication of thin-film SDC electrolytes. Peak power densities of $\sim$525 mW $cm^{-2}$ for SDC-EC cells and 605 mW $cm^{-2}$ for SDC-HT cells were achieved at 600 °C.
(4) Resistance in the cells mainly arose from the electrolyte ohmic drop. Further reduction in electrolyte membrane thickness or increases in the membrane density may be necessary to further increase cell performance at reduced operating temperatures.

## Acknowledgements

This work was supported by the National Natural Science Foundation of China under contract nos. 20703024, and 20676061, by the National 863 Program under contract no. 2007AA05Z133 and by the National Basic Research Program of China under contract no. 2007CB209704.

## References

[1] T. Hibino, A. Hashimoto, T. Inoue, J. Tokuno, S. Yoshida, M. Sano, Science 288 (2000) 2031–2033.
[2] S. de Souza, S.J. Visco, L.C. De Jonghe, Solid State Ionics 98 (1997) 57–61.
[3] Y.M. Choi, M.C. Lin, M.L. Liu, Angew. Chem. Int. Ed. 46 (2001) 7214–7219.
[4] W. Zhou, R. Ran, R. Cai, Z.P. Shao, W.Q. Jin, N.P. Xu, J. Power Sources 186 (2009) 244–251.
[5] Z.P. Shao, S.M. Haile, Nature 431 (2004) 170–173.
[6] W. Zhou, R. Ran, Z.P. Shao, W.Q. Jin, N.P. Xu, J. Power Sources 182 (2008) 24–31.
[7] W. Zhou, Z.P. Shao, R. Ran, H.X. Gu, W.Q. Jin, N.P. Xu, J. Am. Ceram. Soc. 91 (2008) 1155–1162.
[8] M. Shah, S.A. Barnett, Solid State Ionics 179 (2008) 2059–2064.
[9] S.P. Scott, D. Mantzavinos, A. Hartley, M. Sahibzada, I.S. Metcalfe, Solid State Ionics 152–153 (2002) 777–781.
[10] C.R. Xia, W. Rauch, F. Chen, M.L. Liu, Solid State Ionics 149 (2002) 11–19.
[11] L. Yang, C. Zuo, S. Wang, Z. Cheng, M.L. Liu, Adv. Mater. 20 (2006) 3280–3283.
[12] H. Fukunaga, M. Koyama, N. Takahashi, C. Wen, K. Yamada, Solid State Ionics 132 (2000) 279–285.
[13] W. Zhou, R. Ran, Z.P. Shao, R. Cai, W.Q. Jin, N.P. Xu, J. Ahn, Electrochim. Acta 53 (2008) 4370–4380.
[14] T.Z. Sholklapper, V. Radmilovic, C.P. Jacobson, S.J. Visco, L.C. De Jonghe, J. Power Sources 175 (2008) 206–210.
[15] K. Sasaki, K. Hosoda, T.N. Lan, K. Yasumoto, S. Wang, M. Dokiya, Solid State Ionics 174 (2004) 97–102.
[16] Y. Sakito, A. Hirano, N. Imanishi, Y. Takeda, O. Yamamoto, Y. Liu, J. Power Sources 182 (2008) 476–481.
[17] K. Sasaki, J. Tamura, H. Hosoda, T.N. Lan, K. Yasumoto, M. Dokiya, Solid State Ionics 148 (2002) 551–555.
[18] M. Sahibzada, S.J. Benson, R.A. Rudkin, J.A. Kilner, Solid State Ionics 113–115 (1998) 285–290.
[19] J.H. Wang, M.L. Liu, M.C. Lin, Solid State Ionics 177 (2006) 939–947.
[20] L. Baqué, A. Caneiro, M.S. Moreno, A. Serquis, Electrochem. Commun. 10 (2008) 1905–1908.
[21] J. Yoon, R. Araujo, N. Grunbaum, L. Baqué, A. Serquis, A. Caneiro, X.H. Zhang, H.Y. Wang, Appl. Surf. Sci. 254 (2007) 266–269.
[22] W. Zhou, Z.P. Shao, R. Ran, Electrochem. Commun. 10 (2008) 1647–1651.
[23] W. Zhou, Z.P. Shao, R. Ran, W.Q. Jin, N.P. Xu, Chem. Commun. 44 (2008) 5791–5793.
[24] C.H. Wang, W.L. Worrell, S. Park, J.M. Vohs, R.J. Gorte, J. Electrochem. Soc. 148 (2001) A864–A868.
[25] S.W. Zha, A. Moore, H. Abernathy, M.L. Liu, J. Electrochem. Soc. 151 (2004) A1128–A1133.
[26] J.B. Goodenough, Solid State Ionics 94 (1997) 17–25.
[27] J.B. Goodenough, Ann. Rev. Mater. Res. 33 (2003) 91–128.
[28] H. Inaba, H. Tagawa, Solid State Ionics 83 (1996) 1–16.
[29] B.C.H. Steele, A. Heinzel, Nature 414 (2001) 170–173.
[30] K.L. Choy, Prog. Mater. Sci. 48 (2003) 57–170.
[31] O. Unal, T.E. Mitchell, A.H. Heuer, J. Am. Ceram. Soc. 77 (1994) 984–992.
[32] H. Sasaki, S. Otoshi, M. Suzuki, T. Sogi, A. Kajimura, N. Sugiuara, M. Ippommatsu, Solid State Ionics 72 (1994) 253–256.
[33] J.H. Song, S. Park, J.H. Lee, H.S. Kim, J. Mater. Process. Technol. 198 (2008) 414–418.
[34] L. Besra, C. Compson, M.L. Liu, J. Power Sources 173 (2007) 130–136.
[35] W.W. Sun, X.Q. Huang, Z. Lü, L.J. Zhao, B. Wei, S.Y. Li, K.F. Chen, N. Ai, W.H. Su, J. Phys. Chem. Solids 70 (2009) 164–168.
[36] X.S. Xin, Z. Lü, Q.S. Zhu, X.Q. Huang, W.H. Su, J. Mater. Chem. 17 (2007) 1627–1630.
[37] C.R. Xia, M.L. Liu, J. Am. Ceram. Soc. 84 (2001) 1903–1905.
[38] Z.P. Shao, S.M. Haile, J. Ahn, P.D. Ronney, Z.L. Zhan, S.A. Barnett, Nature 435 (2005) 795–798.
[39] E. Schüller, R. Vaßen, D. Stöver, Adv. Eng. Mater. 4 (2002) 659–662.
[40] K. Xie, R.Q. Yan, Y.Z. Jiang, X.Q. Liu, G.Y. Meng, J. Membr. Sci. 325 (2008) 6–10.
[41] W. Zhou, H.G. Shi, R. Ran, R. Cai, Z.P. Shao, W.Q. Jin, J. Power Sources 184 (2008) 229–237.
[42] D. Beckel, A. Bieberle-Hütter, A. Harvey, A. Infortuna, U.P. Muecke, M. Prestat, J.L.M. Rupp, L.J. Gauckler, J. Power Sources 173 (2007) 325–345.
[43] R. Muccillo, E.N.S. Muccillo, F.C. Fonseca, Y.V. Franc, J. Power Sources 156 (2006) 455–460.
[44] B. Lin, W.P. Sun, K. Xie, Y.C. Dong, D.H. Dong, X.Q. Liu, J.F. Gao, G.Y. Meng, J. Alloys Compd. 465 (2008) 285–290.
[45] Y.J. Leng, S.H. Chan, K.A. Khor, S.P. Jiang, Int. J. Hydrogen Energy 29 (2004) 1025–1033.
[46] J. Ding, J. Liu, Solid State Ionics 179 (2008) 1246–1249.
[47] M. Mogensen, N.M. Sammes, G.A. Tompsett, Solid State Ionics 129 (2000) 63–94.
[48] T.S. Zhang, J. Ma, L.B. Kong, P. Hing, Y.J. Leng, S.H. Chan, J.A. Kilner, J. Power Sources 124 (2007) 26–33.
[49] T.S. Zhang, H. Peter, H.T. Huang, J.A. Kilner, J. Mater. Process. Technol. 113 (2001) 463–468.
[50] A. Moure, J. Tartaj, C. Moure, J. Eur. Ceram. Soc. 29 (2009) 2559–2565.

[51] W. Zhou, Z.P. Shao, W.Q. Jin, J. Alloys Compd. 426 (2006) 368–374.
[52] H.B. Li, C.R. Xia, M.H. Zhu, Z.X. Zhou, G.Y. Meng, Acta Mater. 54 (2006) 721–727.
[53] D. Ding, B.B. Liu, Z.N. Zhu, S. Zhou, C.R. Xia, Solid State Ionics 179 (2008) 896–899.
[54] G.B. Balazs, R.S. Glass, Solid State Ionics 76 (1995) 155–162.
[55] W. Huang, P. Shuk, M. Greenblatt, Solid State Ionics 100 (1997) 23–27.
[56] B.C.H. Steele, Solid State Ionics 129 (2000) 95–110.
[57] X.G. Zhang, M. Robertson, C. Deĉes-Petit, W. Qu, O. Kesler, R. Maric, D. Ghosh, J. Power Sources 164 (2007) 668–677.